PL-TR-92-2136

ANALYSIS OF H_2O INFRARED RADIANCE MEASURED DURING THE ELC-1 ROCKET EXPERIMENT

P. De
S. M. Adler-Golden

Spectral Sciences, Inc.
99 South Bedford Street, #7
Burlington, MA 01803

15 May 1992

Scientific Report No. 1

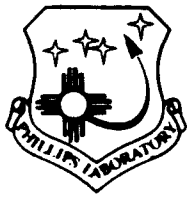

Phillips Laboratory
Directorate of Geophysics
AIR FORCE MATERIEL COMMAND
HANSCOM AIR FORCE BASE, MA 01731-5000

This technical report has been reviewed and is approved for publication.

DEAN F. KIMBALL
Contract Manager
Simulation Branch

WILLIAM A. M. BLUMBERG, Chief
Simulation Branch
Optical Environment Division

ROGER A. VAN TASSEL, Director
Optical Environment Division

This document has been reviewed by the ESC Public Affairs Office (PA) and is releasable to the National Technical Information Service (NTIS).

Qualified requestors may obtain additional copies from the Defense Technical Information Center. All others should apply to the National Technical Information Service.

If your address has changed, or if you wish to be removed from the mailing list, or if the addressee is no longer employed by your organization, please notify PL/IMA, Hanscom AFB, MA 01731-5000. This will assist us in maintaining a current mailing list.

Do not return copies of this report unless contractual obligations or notices on a specific document requires that it be returned.

REPORT DOCUMENTATION PAGE

Form Approved
OMB No. 0704-0188

1. AGENCY USE ONLY (Leave blank)	2. REPORT DATE	3. REPORT TYPE AND DATES COVERED
	15 May 1992	Scientific Report No. 1

4. TITLE AND SUBTITLE
Analysis of H_2O Infrared Radiance Measured During the ELC-1 Rocket Experiment

5. FUNDING NUMBERS
C - F19628-91-C-0083
PE - 63215C
PR - S321
TA - 13
WU - AA

6. AUTHOR(S)
P. De and S. M. Adler-Golden

7. PERFORMING ORGANIZATION NAME(S) AND ADDRESS(ES)
Spectral Sciences, Inc.
99 South Bedford Street, #7
Burlington, MA 01803-5169

8. PERFORMING ORGANIZATION REPORT NUMBER
SSI-TR-213

9. SPONSORING/MONITORING AGENCY NAME(S) AND ADDRESS(ES)
Phillips Laboratory
Hanscom AFB, MA 01731-5000

Contract Manager: Dean Kimball/GPOS

10. SPONSORING/MONITORING AGENCY REPORT NUMBER
PL-TR-92-2136

11. SUPPLEMENTARY NOTES

12a. DISTRIBUTION/AVAILABILITY STATEMENT
Approved for public release; distribution unlimited

12b. DISTRIBUTION CODE

13. ABSTRACT (Maximum 200 words)

This report presents an analysis of selected long-wavelength infrared (LWIR) limb radiance data measured in the ELC-1 radiometer experiment, launched on October 25, 1983 from the White Sands Missile Range, NM at local time 0426 hrs. From the CO_2 ν_2 band emission, information on the mesospheric temperature profile and the radiometer absolute calibration is extracted. The results are combined with a measurement of water vapor rotational emission in the 23-29 μm region to derive a water vapor profile, accurate to within around a factor-of-two range, for 55 km - 85 km altitudes. The ELC-1 results are consistent with previous mid-latitude measurements, made by microwave and solar IR absorption techniques, during fall or early winter months, and are of comparable or better accuracy. These results demonstrate the feasibility of global long-range sensing of water vapor in the mesosphere from rotational emission data obtained in satellite experiments, including the CIRRIS-1A experiment flown on the Space Shuttle STS-39 in April, 1991.

14. SUBJECT TERMS	15. NUMBER OF PAGES
water mesosphere LWIR rotational	26
	16. PRICE CODE

17. SECURITY CLASSIFICATION OF REPORT	18. SECURITY CLASSIFICATION OF THIS PAGE	19. SECURITY CLASSIFICATION OF ABSTRACT	20. LIMITATION OF ABSTRACT
UNCLASSIFIED	UNCLASSIFIED	UNCLASSIFIED	SAR

TABLE OF CONTENTS

LIST OF FIGURES

LIST OF FIGURES (CONTINUED)

LIST OF TABLES

1. INTRODUCTION

This report presents an analysis of selected long-wavelength infrared (LWIR) limb radiance data measured in the 1983 ELC-1 rocket experiment. From the CO_2 ν_2 band emission, information on the mesospheric temperature profile and the radiometer absolute calibration is extracted. The results are combined with a measurement of water vapor rotational emission in the 23-29 μm region to derive a water vapor profile for the altitude range 55 km - 85 km. Over most of these altitudes the emission is optically thick. The methods presented here can also be applied to data obtained in the CIRRIS-1A experiment flown on the Space Shuttle STS-39 in April, 1991,[1] which viewed the earth limb with near-global coverage.

We begin with a brief description of the experiment. In the next section, the temperature profile is discussed. In the subsequent sections, we discuss the data reduction and inversion methods used to derive the water vapor profile. Finally, the ELC-1 water vapor profile is compared to ground-based microwave measurements and to infrared absorption measurements from spacecraft.

The ELC-1 rocket experiment was launched on October 25, 1983 from the White Sands Missile Range, at local time 0426 hours. The geomagnetic activity index Kp for that day was 1.61 and the solar flux index F10.7 was 89. The atmospheric model MSIS-90[2] was run with these inputs to define the profiles used in the data analysis.

The ELC-1 radiometer contained an array of cryogenically-cooled detectors covering the spectral range 4 μm - 29 μm. The basic sensor was previously flown in the Zodiacal Infrared Project (ZIP).[3] For the ELC-1 experiment the sensor was mated to a high-off-axis-rejection telescope, and the detectors were fitted with bandpass filters to yield the spectral responses given in Table 1.

The rocket reached an apogee of 300 km at 296 sec time after launch (TAL). Limb-viewing horizontal, vertical, drop and roll scans were performed during the interval 110 - 478 sec TAL. The aspect solution[4] was obtained by combining star camera and gyroscope data and iterating to obtain self-consistent IR radiance profiles. In this report, data from two sets of

scans are analyzed: a set of four horizontal scans taken during the interval 230 - 256 sec TAL and a set of four vertical scans taken during 353 - 478 sec TAL. Based on the self-consistency of the radiance profiles and the use of the star data to establish the absolute aspect, we estimate the tangent heights to be accurate to within 2 km or better.

The CO_2 $\nu 2$ band emissions were measured by detectors 7, 9 and 31, and the H_2O pure rotational emission was measured by detectors 27 and 28. Other detectors provide useful data on the O_3 $\nu 3$ cold and hot bands in the 9-12 μm region and on the NO fundamental at 5.3 μm. These data will be the subject of a future report.

Table 1. Bandpasses for ELC-1 Detectors for a Blackbody at 300K.

Detector Number	Band Center Wavelength (μm)	Optical Passband (μm)
1,2	15.137	14.76-15.52
3,4	12.498	12.02-12.97
5,6	9.630	9.28-9.98
7,8	16.435	15.79-17.08
9,10	13.747	13.06-14.43
11,12	9.586	9.24-9.93
13,14	10.583	10.02-11.15
15,16	15.180	14.82-15.54
17,18	14.097	13.56-14.63
21,22	5.571	5.11-6.03
23,24	4.653	4.34-4.97
27,28	26.201	23.38-29.02
29,30	11.499	11.00-12.00
31,32	15.197	14.81-15.58

2. TEMPERATURE PROFILE

The inferred H_2O profile is sensitive to the assumed temperature profile. Our approach for determining the temperature profile of the ELC-1 atmosphere was a simple one. The initial density and temperature profiles were taken from the empirical model MSIS-90.[2] For the altitude range of interest (up to 85 km), the CO_2 mixing ratio was set to the value at ground level. The CO_2 spectral radiance profile in the ν_2 region was then calculated using the Strategic High Altitude Radiance Code (SHARC).[5]

The assumed CO_2 density profile should be reasonably accurate, and in any case the radiance is insensitive to it since the CO_2 bands are optically thick. Therefore, the only significant sources of disagreement between the SHARC calculation and the ELC-1 data would be errors in the temperature profile or in the radiometric calibration. A calibration error would cause the radiance profile to be uniformly scaled. Errors in the temperature profile, on the other hand, could cause discrepancies that vary with tangent height.

The bandpass radiances were calculated by SHARC for detectors 7, 9, and 31. Detectors 7 and 9 measured emissions from the hot bands of CO_2 (ν_2) while detector 31 measured the cold band radiance. In Figs. 1-3 the measurements and SHARC predictions are compared. The measured radiances in all three bandpasses disagree with the predictions by up to a factor of 1.8.

Presuming first that the sensor calibration is correct, we estimated the temperature shift necessary to bring the SHARC predictions into agreement with the data. This was done using the approximation, valid for optically thick radiation, that the ratio of the SHARC and observed radiances can be represented by the ratio of blackbody intensities evaluated at the MSIS-90 and the actual temperatures. We calculated the temperature shift as a function of tangent height for each of the three bandpasses, from which we calculated an average shift. The temperature shift thus estimated was not uniform, and is approximated by the following equations:

$$
\begin{aligned}
\Delta T &= 0 && \text{if } h \geq 95 \text{ km} \\
&= 20 && \text{if } h \leq 80 \text{ km} \\
&= 20 - 1.33(h - 80) && \text{if } 80 < h < 95
\end{aligned}
\qquad (1)
$$

where h represents the tangent height.

The SHARC predictions for the CO_2 radiances using the new, shifted temperature profile are plotted in Figs. 1-3. The agreement with the ELC-1 data is much better than with the MSIS-90 profile and we conclude that the modified temperature profile may a be good approximation for the temperature during the ELC-1 flight. The modified temperature profile is shown in Fig. 4 as ELC (temp). For comparison, we also plot the unshifted temperature profile of MSIS-90.

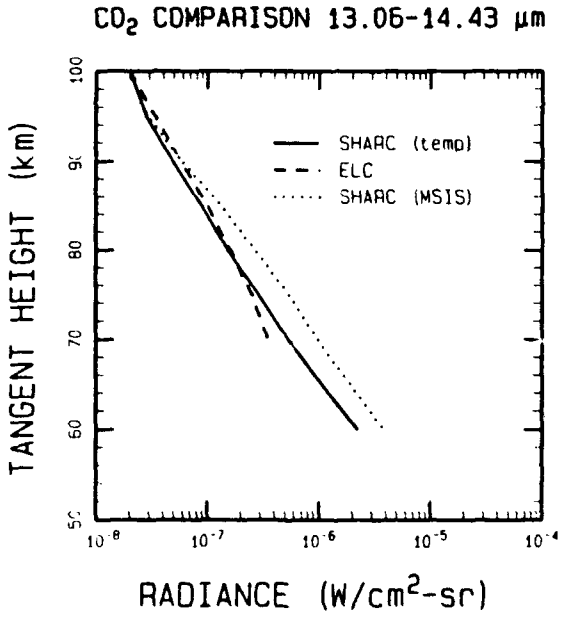

Figure 1. Comparison of CO_2 Radiance Profile From ELC-1 Detector 9 With SHARC Predictions. SHARC (MSIS) Assumes the MSIS-90 Temperature Profile While SHARC (temp) Assumes the Modified Temperature Profile ELC (temp) in Figure 4.

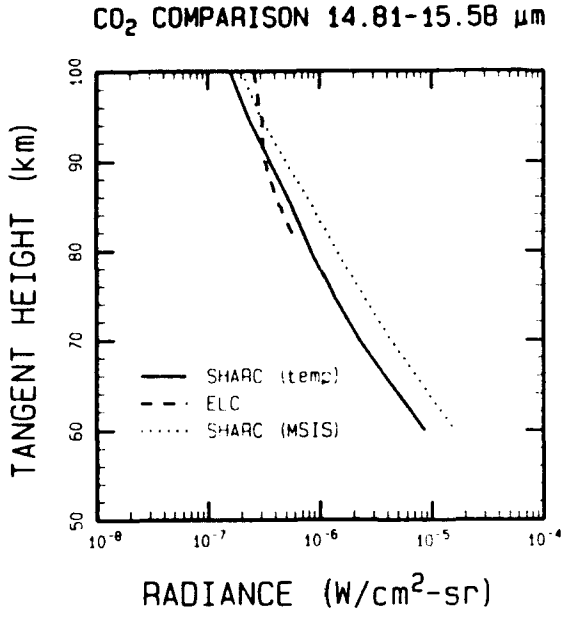

Figure 2. Radiance Profiles as in Figure 1, Except for Detector 31.

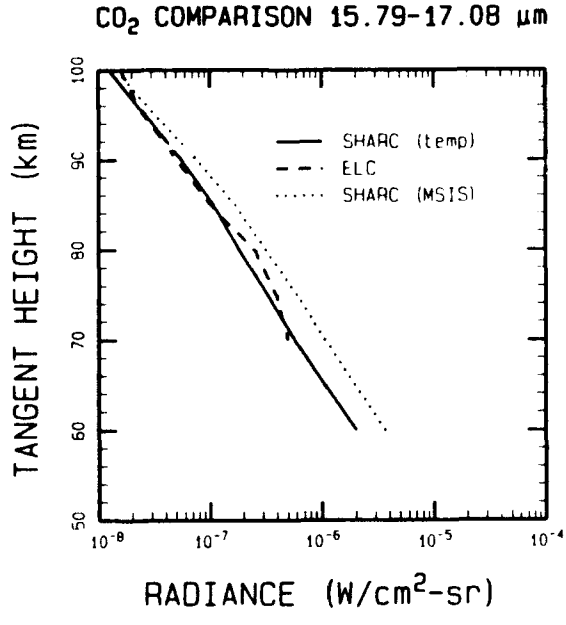

Figure 3. Radiance Profiles as in Figure 1, Except for Detector 7.

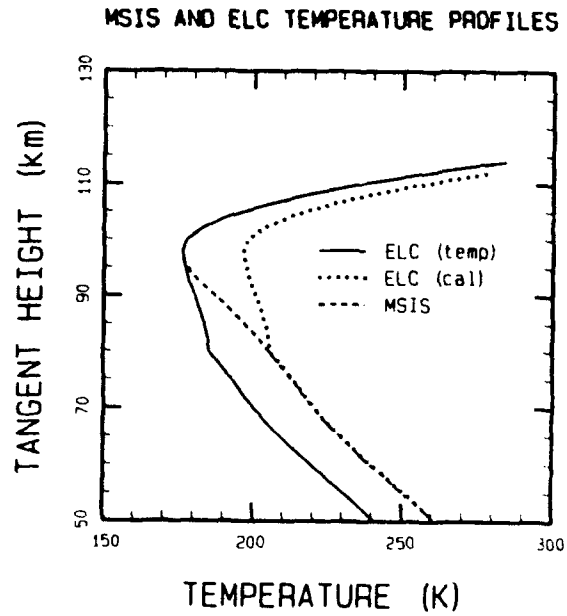

Figure 4. Comparison of Derived Temperature Profiles With the MSIS-90 Profile. ELC (temp) Was Chosen to Match the SHARC Calculation to the Measured CO_2 Radiances. ELC (cal) Was Chosen to Match the Calculation to the Measured Radiances Multiplied by 1.8.

An alternate explanation for the discrepancy between the predicted and observed CO_2 radiances would be a calibration error in the ELC data combined with an error in the kinetic or CO_2 vibrational temperature for altitudes above 80 km. In Fig. 4 we present the kinetic temperature profile needed to match the SHARC radiances predictions to "corrected" data, if we assume that the original ELC data are too low by a factor of 1.8 for all detectors. This profile is labelled as ELC (cal). In Figs. 5-7, we compare the predictions for the ELC (cal) temperature with the recalibrated data. The comparisons are as good as those in Figs. 1-3.

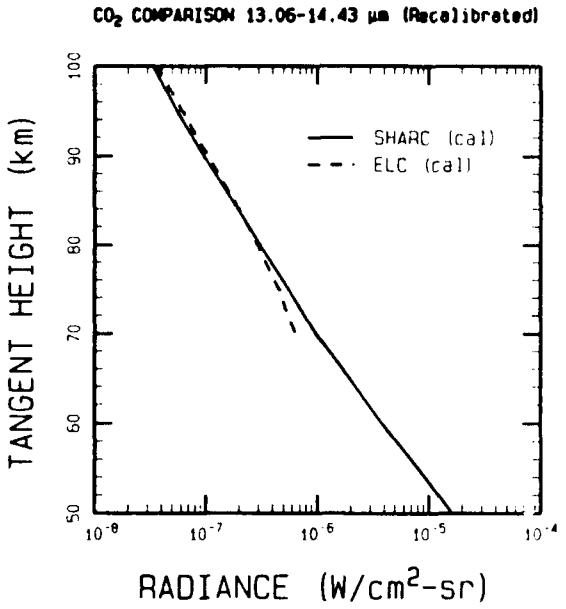

Figure 5. Comparison of 1.8x the CO_2 Radiance Profile From ELC-1 Detector 9 With the SHARC Prediction Based on the Temperature Profile ELC (cal) in Figure 4.

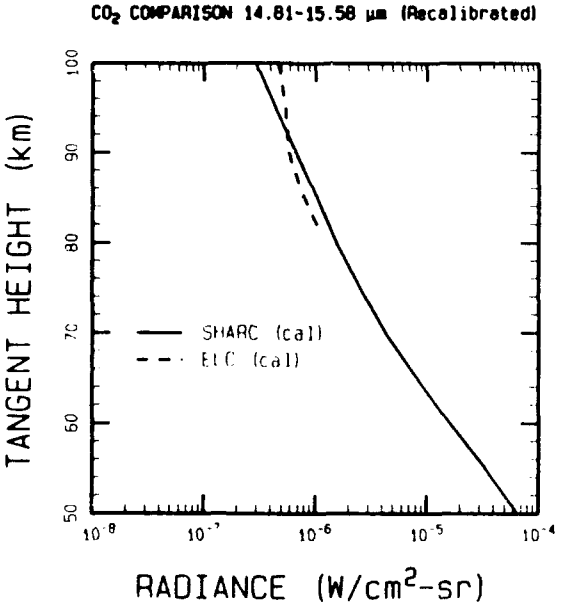

Figure 6. Radiance Profiles as in Figure 5, Except for Detector 31.

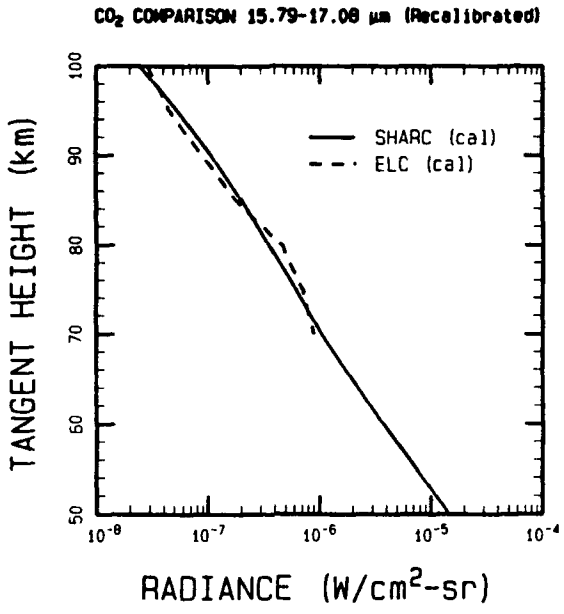

Figure 7. Radiance Profiles as in Figure 5, Except for Detector 7.

The accuracy of the calibration of the similar ZIP instrument has been discussed by Murdock and Price.(3) Based on their discussion, we believe that the proposed calibration correction factor of 1.8 should be an upper limit. We also believe that the alternative possibility of a temperature shift of up to 20° C compared to MSIS-90 would represent an upper limit to the shift, given the typical accuracy of MSIS-90. Therefore, the two temperature profiles in Fig. 4 are most likely the upper and lower bounds for the true ELC temperature profile. These two temperature profiles are used in the subsequent data analysis to provide two separate estimates for the water vapor profile.

3. H_2O DATA REDUCTION

In this section we discuss the procedure by which the raw water vapor data were reduced. Pure rotational emission from H_2O was measured by detectors 27 and 28 in the 23 μm - 29 μm region. We selected two sets of data, one each from the sets of horizontal and vertical scans mentioned earlier. The original data were tabulated in time intervals of 0.003 sec. In order to reduce the data points to a reasonable number, as well as to smooth out some noise, the data were averaged over three time steps. The maximum change in tangent height in this time interval is around 1 km.

The next step in the analysis was to subtract off the background radiance arising from off-axis telescope leakage. This subtraction affects only the highest-altitude water data (above around 80 km). Assuming that above 110 km the signals in the H_2O detectors are entirely due to the leakage background, which decreases exponentially with tangent height, the magnitudes and scale heights for the background were established for each detector. The data for detectors 27 and 28 after the background subtraction are shown in Figs. 8-9.

With the background subtracted, the four sets of data (two each from the two detectors) were averaged. The results, which are shown in Fig. 10 for the limiting calibration scale factors of 1.0 and 1.8, were used in all subsequent analysis. The profile is very smooth, since there were sufficient data at all tangent heights of interest and the signal-to-noise ratio is high.

If the H_2O radiation were optically thin, we could analyze the Fig. 10 profiles using linear techniques such as Abel inversion[6] or a simple onion-peel inversion. However, as discussed in the next section, H_2O is optically thick below 85 km, complicating the inversion process.

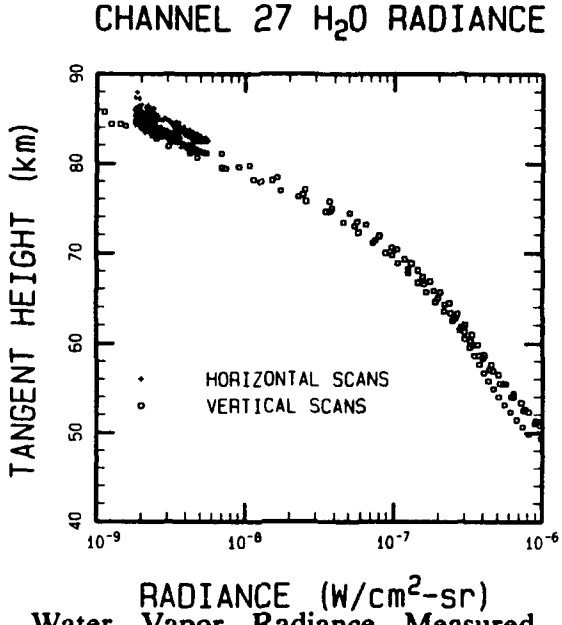

Figure 8. ELC-1 Water Vapor Radiance Measured by Detector 27, After Background Subtraction.

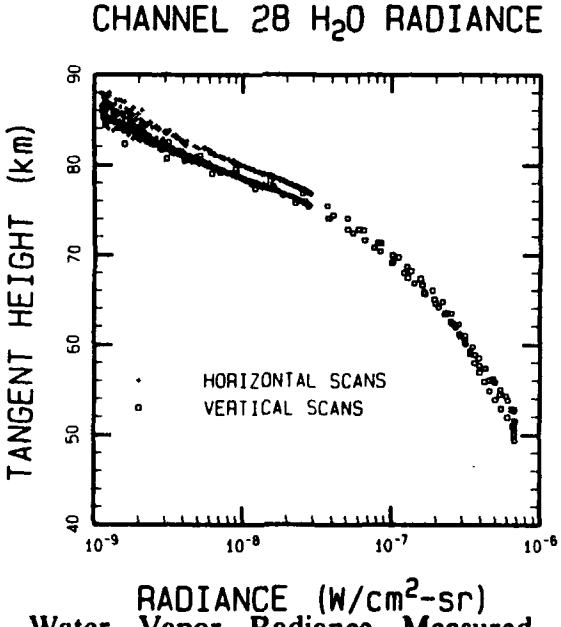

Figure 9. ELC-1 Water Vapor Radiance Measured by Detector 28, After Background Subtraction.

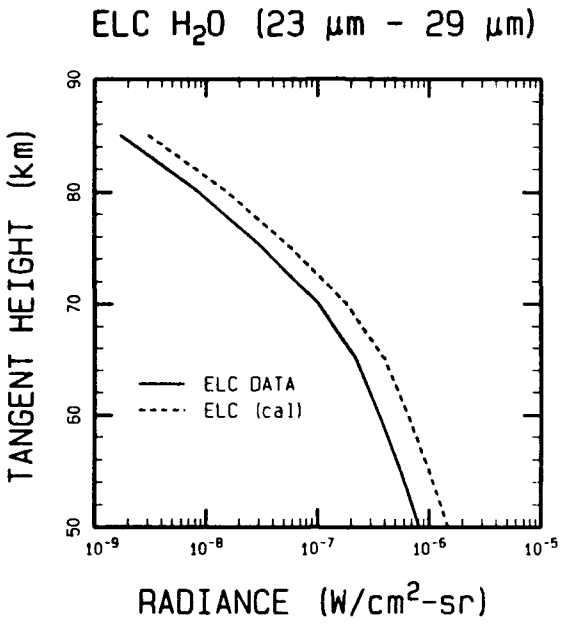

Figure 10. Average ELC-1 Water Vapor Radiance With and Without the Scale Factor of 1.8.

4. WATER VAPOR PROFILE

In order to determine the opacity of H_2O emissions, we ran SHARC for the ELC-1 temperatures and the standard SHARC water vapor density profile. At altitudes above 85 km, the ratio of the full-limb radiance to the half-limb radiance was approximately 2, indicating optically thin emissions. Below 85 km, the ratio of full-limb to half-limb radiances decreased monotonically to almost unity at 50 km, indicating strong self-absorption.

4.1 Inversion Procedures for Optically Thick Emission

The problem of inverting an optically thick limb emission profile is essentially a non-linear fitting problem and may be solved by the usual Newton-Raphson method.(7) The atmosphere is approximated with discrete layers, and a Taylor expansion of the limb radiance is made about an initial-guess profile and truncated after the linear terms. The resulting linear equations are solved and the process is iterated until convergence is achieved. To reduce the dynamic range of the variables, and ensure that errors are expressed in proportional rather than in absolute terms, we may express the number density and limb radiance logarithmically. Then the linear equations are given by

$$\ln(I_j) = \ln(I_{oj}) + \sum_i (d\ln(I_j)/d\ln(N_i))\Delta\ln(N_i) \qquad (2)$$

Here j is the index for the line-of-sight (LOS), I_j is the limb radiance value to be fitted, I_{oj} is the limb radiance calculated using trial densities N_{oi} in each layer i, N_i is the density in layer i, and $\Delta\ln(N_i) \equiv \ln(N_i)-\ln(N_{oi})$. The species density may refer to either ground state or excited state number density, if it is assumed that the relationship between them is governed by a known kinetic, vibrational, or other temperature in each layer.

The partial derivatives in Eq. (2) correspond to the usual weighting functions and may be computed by incrementing the layer densities that are input to the radiation code. The N_i are obtained by solution of the

simultaneous equations, which can be performed by successive substitution starting from the top layer. To achieve convergence, successive iterations can be performed using the N_i as the new trial values N_{oi}.

In the current SHARC code, it is not possible to increment the layer densities without generating a new population file, which requires re-executing the chemistry and radiation transport (CHEMKIN and NEMESIS) routines. Determination of the weighting functions in this manner would be very cumbersome and time-consuming. However, an external or internal routine could be developed to automatically update the population file and execute the LOS radiance computation alone.

For the present application, we have chosen a simpler inversion approach that minimizes the computational effort and uses only the existing SHARC code. Accurate forward calculations are performed for each trial profile, while the partial derivatives that drive successive iterations are approximated using the crude assumption that the distribution of the species column density along the LOS is immaterial. This would be the case if all temperatures (kinetic, vibrational, etc.) were uniform along the LOS. We can then replace Eq. (2) by

$$\ln(I_j) = \ln(I_{oj}) + (d\ln(I_j)/d\ln(N_j))\Delta\ln(N_j) \qquad (3)$$

where N_j is the column density along the j'th LOS and $\Delta\ln(N_j) \equiv \ln(N_j)-\ln(N_{oj})$, N_{oj} being the trial column density. From Eq. (3), the N_i are given by

$$N_j = N_{oj}(I_j/I_{oj})^{1/\alpha_j} \qquad (4)$$

where $\alpha_j \equiv d\ln(I_j)/d\ln(N_j)$. The N_j can be inverted to determine the layer densities N_i using a standard linear inversion method. For optically thin radiation, $\alpha = 1$ and this method reduces to a linear inversion of the column radiance. For optically thick radiation, $\alpha < 1$, which implies that for a given fractional change in species density the associated fractional change in limb radiance is smaller.

The α_j can be determined from only two sets of SHARC calculations with different column density profiles, such as full-limb calculations using

Table 2. Values of $\alpha_j = d\ln(I_j)/d\ln(N_j)$, Where N_j is Water Vapor Column Density Along the LOS.

Tangent Ht (km)	Half-Limb Method (Standard Profile)	Full-Limb Method (Standard and First Iteration Profiles)
≥ 90	1.00	1.00
85	0.97	0.97
80	0.80	0.89
75	0.53	0.68
70	0.36	0.44
65	0.25	0.34
60	0.19	0.37
55	0.18	0.38
50	0.23	0.46

successive density profile iterations or full-limb and half-limb calculations using the same density profile. We used values derived via the half-limb method, which requires only a single CHEMKIN and NEMESIS calculation, to determine the first-iteration profile, and used this profile and the original guess to derive refined α values that were used in subsequent iterations. The α values from both methods are given in Table 2.

Due to the uniform-LOS-temperature assumption in the above inversion scheme, the procedure may not be fully convergent for realistic atmospheres. However, the error can be minimized by a judicious definition of N. For example, if the emission is due to a vibrationally excited state, choosing N as that state rather than the ground state removes the first-order error in the optically thin limit. For the present case of rotationally excited states, we define N as an "effective" excited state species column density,

$$N_j = \sum_i N_i l_{ij} \exp(-E_a/kT_i) \qquad (5)$$

E_a is the average excited state energy (approximately 1100 cm^{-1} for the strong water rotation lines in the ELC-1 bandpass), T_i is the temperature in layer i, l_{ij} is the length of the LOS through layer i, and N_i is the water vapor number density in layer i.

In conclusion, the inversion procedure given by Eqs. (3)-(5) should provide accurate solutions in optically thin conditions (α = 1) as well as with a uniform temperature profile in optically thick conditions. As shown in the following subsection, good results have been obtained in the current investigation of water vapor rotational emission. However, complete convergence under general conditions may require a fuller treatment such as given by Eq. (2). The development of an inversion algorithm along these lines utilizing the SHARC code would be very desirable for future work.

4.2 Application to ELC-1 Water Vapor Data

The inversion procedure based on Eqs. (3)-(5) was implemented using the ELC-1 limb radiance profiles in Fig. 10. With one or two iterations, convergence of the observed and calculated radiances was obtained to within 10% or better at all tangent heights from 55 km to 85 km. The results are shown in Figs. 11-12. In Fig. 11, the comparison is to the predicted radiance for the temperature profile labelled ELC (temp) in Fig. 4. In Fig. 12, the comparison is for the temperature profile labelled ELC (cal). In both comparisons, the agreement is excellent. It is not clear whether the residual error is due to a shortcoming of the inversion method itself or its method of implementation. The comparisons between the calculated and observed radiances in Eq. (4) were made at 5 km tangent height increments, while the SHARC code uses 2-km layering. Given the very small scale height of water vapor emissions, finer altitude grids may ultimately be required.

In Fig. 13, we compare the two ELC-1 water vapor density profiles (for the two temperature profiles) to the SHARC standard profile. At the lower altitudes, the true density profile should lie between the two profiles shown. At higher altitudes, the profiles coalesce. However, there the effect of tangent height uncertainty must be included in an overall error estimate. From the data in Fig. 9, a 2 km tangent height spread is associated with a radiance spread of nearly a factor of 2, and, at these altitudes, a comparable uncertainty in water density. Considering the temperature, tangent height and inversion uncertainties, reasonable bounds for the true water vapor profile in ELC are obtained by averaging the two profiles and taking factor-of-two error bars at all altitudes. The result, expressed as a mixing ratio, is plotted as the shaded area in Figs. 14 and 15.

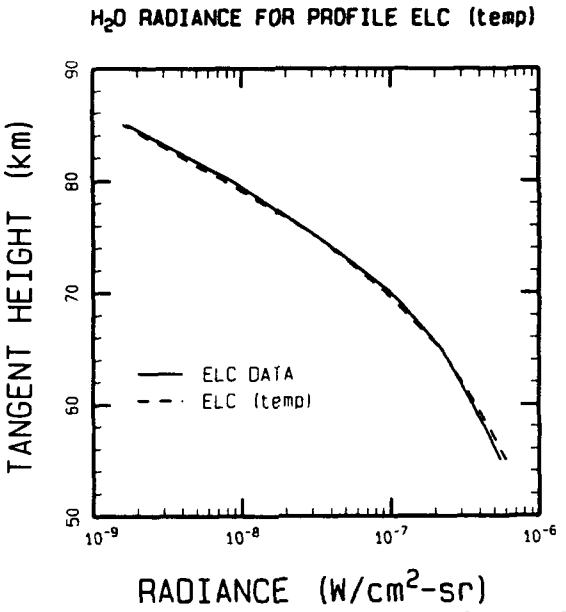

Figure 11. Comparison of Measured Water Vapor Radiance Profile With the SHARC Simulation Using the Density Profile ELC (temp) in Figure 13.

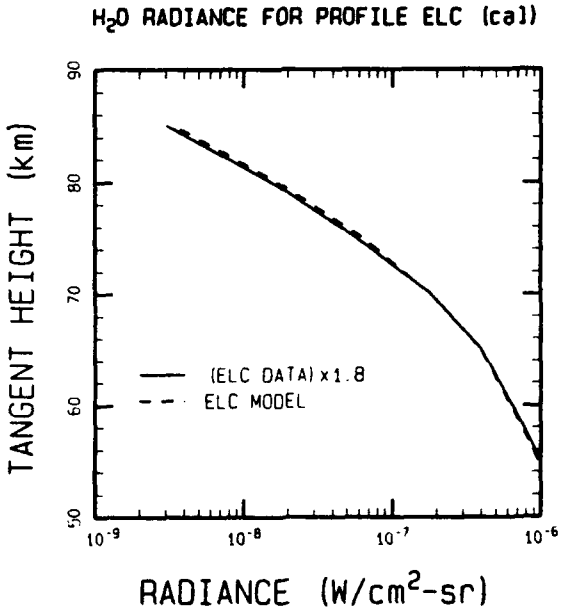

Figure 12. Comparison of Measured Water Vapor Radiance Profile, Including the Scale Factor of 1.8, With the SHARC Simulation Using the Density Profile ELC (cal) in Figure 13.

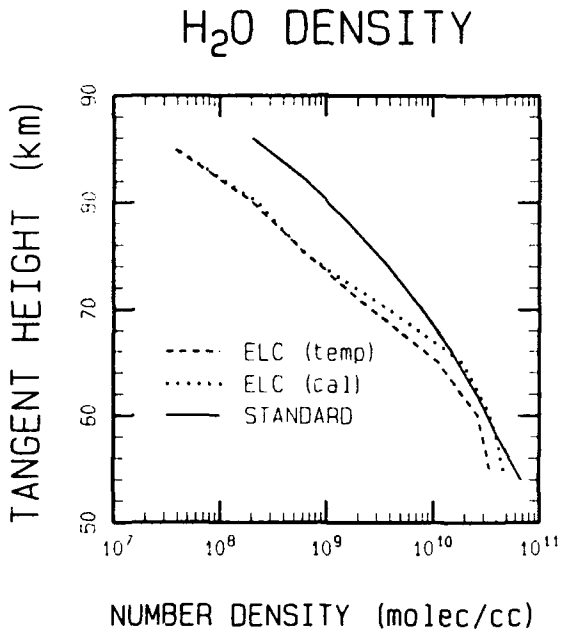

Figure 13. Comparison of the ELC-1 Water Vapor Profiles and the SHARC "Standard" Profile.

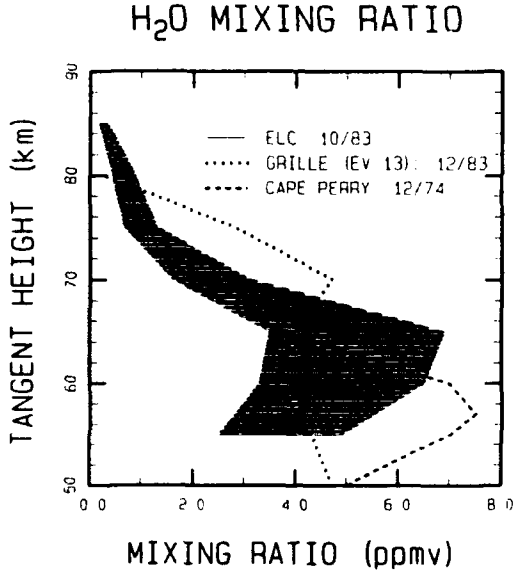

Figure 14. Comparison of the ELC-1 Water Vapor Mixing Ratio (Shaded Area) to Space-Based IR Absorption Measurements Made During the Fall/Winter Months.

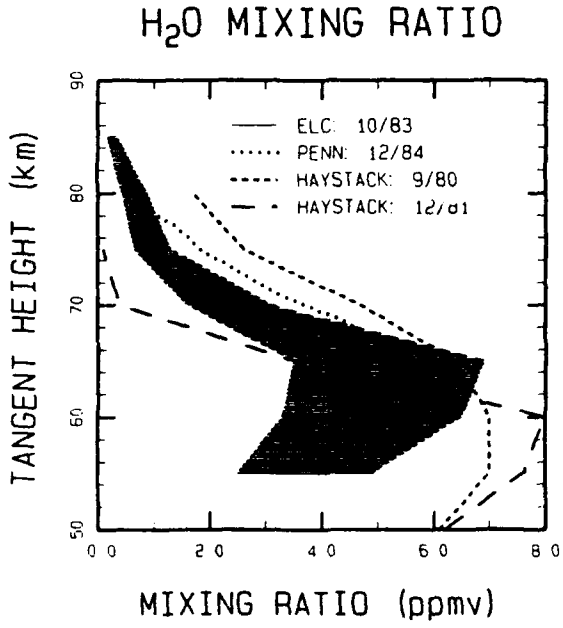

Figure 15. Comparison of the ELC-1 Water Vapor Mixing Ratio (Shaded Area) to Ground-Based Microwave Measurements Made During the Fall/Winter Months.

5. CONCLUSIONS

In Fig. 14 the ELC-1 water vapor profile is compared with measurements from three ground-based microwave experiments at mid-latitudes. These determinations are based on analysis of the 22.2 GHz emission line shape, and are limited to altitudes below 70-80 km.[8] The microwave measurements were made at three different sites: Haystack Observatory in Westford, MA,[9] JPL,[10] and Penn. State.[11] Measurements have been made at various times of the year and a significant seasonal variation has been observed. The water vapor mixing ratio has been seen to vary by an order of magnitude at the higher altitudes and by about a factor of two at the lower altitudes, and is greatest during the late summer months.

In Fig. 15 we compare the ELC-1 result to two other measurements from space platforms. These were made during the first Spacelab mission on board the Space Shuttle, in the winter of 1983[12] and from a rocket launched from Cape Perry on December 6, 1974.[13] In both experiments, the solar absorption spectrum of the 2.7 μm band of water vapor was measured during sunrise or sunset.

Figures 14 and 15 show that the water vapor profile derived from the ELC-1 data is consistent with previous mid-latitude measurements made during fall or early winter months. The uncertainty in an individual profile is about a factor of two and the reader is referred to the original reportings for the exact uncertainties. The range of these measurements, while substantial, is much smaller than for measurements that are not selected according to season.

The results from ELC-1 demonstrate that optically thick rotational emission can be analyzed to yield the altitude profile for water vapor in the mesosphere with an accuracy comparable to microwave and IR absorption methods. Global data from CIRRIS-1 can be analyzed in a similar manner and can be expected to provide valuable information for understanding and modeling water vapor's variability.

Acknowledgements

The authors thank Donald Smith, Steven Price, and Anthony D'Agati (Phillips Laboratory) for their assistance in this project and the Air Force for support under Contract No. F19628-91-C-0083.

6. REFERENCES

1. D. R. Smith, W. A. M. Blumberg, R. M. Nadile, S. J. Lipson, E. R. Huppi, and N. B. Wheeler, "Observation of High K Hydroxyl Pure Rotational Lines in Atmospheric Emission Spectra by the CIRRIS 1A Space Shuttle Experiment," Geophys. Res. Lett., 19, 593 (1992).

2. A. E. Hedin, "Extension of the MSIS Thermospheric Model Into the Middle and Lower Atmosphere," J. Geophys. Res., 96, 1159 (1991).

3. T. L. Murdock and S. D. Price, "Infrared Measurements of Zodiacal Light," Astron. J., 90, 375 (1985).

4. A. J. Mazzella, J. R. Palys, W. A. Smith, and S. A. Lacaire, "ELC-1 Aspect Solution," RDP Technical Report 8505, RDP Incorporated (1986).

5. R. D. Sharma, A. J. Ratkowski, R. L. Sundberg, J. W. Duff, L. S. Bernstein, P. K. Acharya, J. H. Gruninger, D. C. Robertson, and R. J. Healey, "Description of SHARC, the Strategic High-Altitude Radiance Code," GL-TR-89-0229, Environmental Research Papers, No. 1036 (1989). ADA213806

6. A. S. Zachor and R. D. Sharma, "Retrieval of Non-LTE Vertical Structure From a Spectrally Resolved Infrared Limb Radiance Profile," J. Geophys. Res., 90, 467 (1985).

7. E. R. Westwater and O. N. Strand, "Inversion Techniques," Chapter 16 in Remote Sensing of the Troposphere, V. E. Derr, Ed., U. S. Dept. of Commerce, NOAA (U. S. Govt. Printing Office, Washington, DC, 1972).

8. E. Kopp, "Hydrogen Constituents of the Mesosphere Inferred From Positive Ions: H_2O, CH_4, H_2CO, H_2O_2, and HCN," J. Geophys. Res., 95, 5613 (1990).

9. R. M. Bevilacqua, J. J. Wilson, P. R. Schwartz, C. J. Gibbins, J. M. Bologna, and D. J. Thacker, "An Observational Study of Water Vapor in the Mid-Latitude Mesosphere Using Ground-Based Microwave Techniques," J. Geophys. Res., 88, 8523 (1983).

10. R. M. Bevilacqua, W. J. Wilson, and P. R. Schwartz, "Measurements of Mesospheric Water Vapor in 1984 and 1985: Results and Implications for Middle Atmospheric Transport," J. Geophys. Res., 92, 6679 (1987).

11. R. M. Bevilacqua, J. J. Olivero, and C. L. Croskey, "Mesospheric Water Vapor Measurements from Penn State: Monthly Mean Observations (1984-1987)," J. Geophys. Res., 94, 12807 (1989).

12. A. Girard, J. Besson, D. Brard, J. Laurant, M. P. Lemaitre, C. Lippens, C. Muller, J. Vercheval, and M. Ackerman, Global Results of GRILLE Spectrometer Experiment On Board Spacelab I," Planet. Space Sci., 36, 291 (1988).

13. R. S. O'Brien and W. F. J. Evans, "Rocket Measurements of the Distribution of Water Vapor in the Stratosphere at High Latitudes," J. Geophys. Res., 86, 12101 (1981).